Micellar Sphere-to-Rod Transition in an Aqueous Triblock Copolymer System. A Dynamic Light Scattering Study of Translational and Rotational Diffusion

Karin Schillén, Wyn Brown,* and Robert M. Johnsen

Department of Physical Chemistry, University of Uppsala, Box 532, S-751 21 Uppsala, Sweden

Received April 4, 1994; Revised Manuscript Received June 11, 1994®

ABSTRACT: In dilute water solutions of a PEO–PPO–PEO triblock copolymer, polarized dynamic light scattering measurement data reveal a sphere-to-rod transition in the shape of the micelles at a temperature close to 70 °C. This transition is anticipated from theory and was also inferred from earlier small-angle neutron scattering measurements. Regularized inverse Laplace transformation of the polarized dynamic light scattering data typically showed a fast rotational diffusion component of low amplitude in addition to a major slow component from translational diffusion. Good agreement was obtained between the rotational diffusion coefficient estimated from the polarized measurements and the value measured directly using depolarized dynamic light scattering. From the rotational diffusion coefficient a length of the P-85 rodlike micelle can be estimated, via Broersma's expressions for the rigid rod, as 1050 Å in the dilute limit. This corresponds to a length/diameter ratio of 7. Intensity autocorrelation functions were modeled on the measured dynamic light scattering data using Pecora's theoretical expressions for the time correlation function in terms of the dynamic form factors. Good agreement between theory and experiment was found at the lowest concentrations. Concentrations $c > 0.05\%$ correspond to the semidilute regime where interparticle friction effects preclude determination of the length.

Introduction

Triblock copolymers of poly(ethylene oxide) and poly(propylene oxide) (PEO–PPO–PEO) are nonionic low molecular weight amphiphilic substances (surfactants) which have received much attention in the literature due to their complex aggregation behavior in aqueous solution; see, for example, refs 1–4. The present article deals with a triblock copolymer (denoted P-85) which is described under Materials. With both P-85 and structurally similar copolymers, an increase in temperature leads to micelle formation driven by the hydrophobic PPO block. The micelle formation closely resembles the behavior of conventional surfactants which follow a closed association mechanism where there is an equilibrium between the monomers (here the molecular copolymers) and micelles.[5,6] The micelles form over a broad range in temperature and a sharp critical micelle concentration is not observed, probably owing to polydispersity in the constituents of the copolymer. At lower temperatures, the micelles are known to have spherical symmetry with a compact liquidlike core of water-insoluble PPO blocks and an outer corona formed by the soluble PEO blocks swollen by water. Theoretical calculations have indicated that the core also has a low water content and some of the PEO component.[7] Pulsed field gradient NMR measurements[8] indicate that in the 1–10% (w/w) concentration region the aggregation number of the spherical micelle apparently does not depend on the copolymer concentration and that the lifetime of a monomer in the micelle is between 10 μs and 1 ms. The core radius obtained from hard-sphere analysis of small-angle neutron scattering (SANS) data[9] also appeared to be independent of copolymer concentration.

Phase diagrams of the triblock copolymer P-85 and related block copolymers in aqueous solution have been presented based on small-angle neutron scattering data[9] and mean-field lattice theory.[10] Recently, modifications to the phase diagram for P-85 have been made based on small-angle X-ray scattering (SAXS), ultrasonic speed measurements, differential scanning calorimetry, low shear viscometry, and light transmission experiments.[11] The phase diagram shows the existence of a solution of free monomers and a region with spherical micelles forming over a broad micellization regime. At higher concentrations ($c > 25\%$ (w/w)) and elevated temperatures, a regime with very high viscosity and viscoelastic behavior exists. This transition to a stiff, hard gel has been investigated using several techniques.[11–14] SANS measurements showed that the gel regime is an ordered structure due to close packing of micelles in a cubic (bcc) pattern. At even higher temperatures a hexagonal phase is present.

In the more dilute region, the spherical micelles are replaced at higher temperatures by a soft gel, presumably resulting from the interaction between rodlike micelles. It is our intention here to attempt to further elucidate the influence of temperature. Recent results from SANS measurements[9] have been interpreted as showing that the spherical micelles of P-85 grow as the temperature increases and that the shape changes progressively to an elongated structure commencing at about 65–70 °C. There is also a strong theoretical prediction for a sphere-to-rod transition in these block copolymer systems based on model calculations of phase diagrams using a mean-field lattice theory for heterogeneous systems.[10] Pulsed field gradient NMR results also show a growth of the P-85 micelles with increasing temperature (above 70 °C).[8] From preliminary optical microscopy studies a micellar sphere-to-rod transition is also indicated.[15] It was therefore of interest to see if this transition could be detected using dynamic light scattering (DLS).

Polarized (VV) and depolarized (VH) DLS measurements are reported here on the P-85 system in the higher temperature range (70–90 °C) over which the sphere-to-rod transition was anticipated to occur. Several approaches are used to derive estimates of the micellar length from the scattering data.

* Abstract published in *Advance ACS Abstracts*, July 15, 1994.

0024-9297/94/2227-4825$04.50/0 © 1994 American Chemical Society

Theory

Pecora[16] showed that for optically isotropic rods the normalized electric field correlation function, $g^{(1)}(t)$, may be expanded to consist of a weighted sum of two (or more) exponential decays, where the first is the purely translational part and the second is related to the rotational diffusion about the center of mass of the rod:

$$g^{(1)}(t) = S(q,t) = S_0(qL)\exp(-q^2Dt) + S_1(qL)\exp(-(q^2D + 6\Theta)t) + \dots \quad (1)$$

Here $q = 4\pi n \sin(\theta/2)/\lambda$ is the magnitude of the scattering vector where n, θ, and λ are the refractive index of the medium (approximated to the solvent), the scattering angle, and the incident wavelength, respectively. D is the translational diffusion coefficient, L is the rod length, and Θ is the rotational diffusion coefficient. $S(q,t)$ is the dynamic form factor which gives the wave vector dependence of the total scattered light intensity for an isotropic rodlike molecule. The scattering amplitudes (weighting factors), $S_0(qL)$ and $S_1(qL)$, may be calculated using standard relationships:

$$S_0(qL) = \left(\frac{2}{qL}\int_0^{qL/2}\frac{\sin z}{z}\,dz\right)^2 \quad (2a)$$

$$S_1(qL) = 5\left[(qL)^{-1}\left(-3j_1(qL/2) + \int_0^{qL/2}\frac{\sin z}{z}\,dz\right)\right]^2 \quad (2b)$$

where $j_1(qL/2)$ is the spherical Bessel function of order 1.

In the angular region where $qL < 3$, the only motion that will contribute significantly to the dephasing of the scattered light for a rod of length L is translational motion, and as qL becomes greater, the rotation of the rod increasingly contributes. In the limit of very low qL, the relaxation time distribution is thus composed of a single translational decay mode, of rate Γ_s. At $qL > 3$, the amplitude, $S_1(qL)$, of the second decay (Γ_f) becomes sufficiently large that it is possible to estimate the rotational diffusion coefficient (Θ) from DLS measurements. Since the sum of the terms higher than those shown in eq 1 is negligible for $qL < 8$, then

$$6\Theta = \Gamma_f - q^2D \quad (3)$$

and the quantity Θ can be obtained directly in the low-angle limit, $q \to 0$. At inifinite dilution, Θ and D for rigid noninteracting rods with $L/d > 5$ can be expressed by Broersma's relationships:[17-19]

$$\Theta = \left(\frac{3kT}{\pi\eta_0 L^3}\right)(\delta - \zeta)$$

$$\delta = \ln(2L/d) \quad (4)$$

$$\zeta = 1.45 - 7.5(1/\delta - 0.27)^2$$

$$D = \left(\frac{kT}{3\pi\eta_0 L}\right)(\delta - 0.5(\gamma_\parallel + \gamma_\perp))$$

$$\gamma_\parallel = 1.27 - 7.4(1/\delta - 0.34)^2 \quad (5)$$

$$\gamma_\perp = 0.19 - 4.2(1/\delta - 0.39)^2$$

where L is the length of the rod of diameter d and η_0 is the viscosity of the solvent. A long rod will have anisotropic translation resulting in a coupling between translation and rotation.[18] In the case of short rods the anisotropy, $\Delta D = D_\parallel - D_\perp$, is small:[19]

$$D_\parallel = \frac{kT}{2\pi\eta_0 L}(\delta - \gamma_\parallel) \quad (6a)$$

$$D_\perp = \frac{kT}{4\pi\eta_0 L}(\delta - \gamma_\perp) \quad (6b)$$

where δ, $\gamma_\parallel$, and $\gamma_\perp$ are given in eqs 4 and 5.

Experimental Section

Materials. The triblock copolymer, Synperonic P-85, obtained from Serva AG in Heidelberg, Germany, has a formal number-average molecular weight of 4600. The structural formula for the average composition is $HO(C_2H_4O)_{27}(C_3H_6O)_{39}(C_2H_4O)_{27}H$, where $(C_2H_4O)_{27+27}$ is 50% of the total weight of the compound. P-85 was purified by an extraction procedure with hexane[20] in an endeavor to remove the contamination of the poly(propylene oxide)-rich species.

Water solutions of P-85 with concentrations of 0.025, 0.050, 0.10, 0.50, and 1.0% (w/w) were individually prepared at 6 °C. They were filtered, also at 6 °C at which the solutions are monomeric, through 0.22-μm Millipore filters with Durapore membranes into 10-mL cylindrical ampules and flame-sealed under a N_2(g) atmosphere.

Dynamic Light Scattering Measurements. The scattering cells (10-mL sealed cylindrical ampules) were immersed in a large-diameter thermostated bath of index-matching liquid (silicone oil). The polarized (VV) DLS measurements in the self-beating (homodyne) mode were performed using a frequency-stabilized Coherent Innova Ar ion laser operating at 488 nm with adjustable output power. A typical laser power was 25 mW for the polarized data of the higher concentrations. The light was vertically polarized with a Glan-Thompson polarizer, with extinction better than 10^{-6}.

The detector optics employed a 4-μm-diameter monomodal fiber coupled to an ITT FW130 photomultiplier, the output of which was digitized by an ALV-PM-PD amplifier–discriminator. The signal analyzer was an ALV-5000 digital multiple-τ correlator (Langen GmbH) with 288 exponentially spaced channels. It has a minimum real time sampling time of 0.2 μs and a maximum of about 100 s. The intensity autocorrelation function, $g^{(2)}(t)$, was measured at different angles. In the present study, in most cases, the temperature was 75 °C and was controlled to within ±0.02 °C.

Measurements of depolarized dynamic light scattering were also made where the scattered light passed through a Glan-Thompson polarizer with an extinction coefficient better than 10^{-7} whose orientation was adjusted to give the minimum intensity for a dilute solution of a high molecular weight polystyrene in ethyl acetate.

Data Analysis. The DLS data were analyzed by nonlinear regression procedures. The various models used in the fitting procedures are expressed with respect to $g^{(1)}(t)$, while the fitting was performed with respect to the measured $g^{(2)}(t)$, described as

$$g^{(2)}(t) - 1 = \beta|g^{(1)}(t)|^2 \quad (7)$$

where β is a nonideality factor which accounts for the deviation from ideal correlation.

$g^{(1)}(t)$ can be written as the Laplace transform of the distribution of relaxation rates, $G(\Gamma)$:

$$g^{(1)}(t) = \int_0^\infty G(\Gamma)\exp(-\Gamma t)\,d\Gamma \quad (8)$$

where Γ is the relaxation rate and t is the lag time. For relaxation times, τ, eq 8 will be expressed as

$$g^{(1)}(t) = \int_0^\infty \tau A(\tau)\exp(-t/\tau)\,d\ln\tau \quad (9)$$

where $\tau A(\tau) \equiv \Gamma G(\Gamma)$ in the logarithmic scale. $\tau A(\tau)$ was obtained by regularized inverse Laplace transformation (RILT) of the dynamic light scattering data using a constrained regularization calculation algorithm called REPES[21-23] as incorporated in the analysis package GENDIST (see Appendix). This algorithm

directly minimizes the sum of the squared differences between experimental and calculated $g^{(2)}(t)$ functions. It allows the selection of a "smoothing parameter", *probability to reject*—the higher the *probability to reject*, the greater the smoothing. A value of 0.5 was chosen as standard in all analyses.

Analysis was also made using a double-exponential function as a $g^{(1)}(t)$ model:

$$g^{(1)}(t) = A_2 \exp(-t/\tau_1) + A_2 \exp(-t/\tau_2) + baseline \quad (10)$$

where τ_1 and τ_2 are the average relaxation times for the two decays. The A's are the amplitudes.

All the polarized DLS measurements were also analyzed using a program which constructs an intensity autocorrelation function based on a rodlike particle model. The rod model will be described as follows, where eq 7 is used together with eq 11 (see also eq 1):

$$g^{(1)}(t) = S_0 \exp(-\Gamma_s t) + S_1 \exp(-\Gamma_f t) + baseline \quad (11)$$

The length of the rod may be estimated by nonlinear least squares fitting to the experimental $g^{(2)}(t) - 1$ function.

The first approach was to determine β and the baseline in a preliminary RILT calculation. Subsequently, the L value, which yields the best fit of the $g^{(2)}(t) - 1$ function calculated from eqs 11 and 7 via Broersma's equations (eqs 4 and 5), is determined. S_0, S_1, Γ_s, and Γ_f are all calculated from L and q using, respectively, eq 2a, eq 2b, $\Gamma_s = q^2D$, and eq 3. Such nonlinear fitting with only one variable is most easily performed with a "Golden Section Search" routine[24] which requires as input two L values which bracket the minimum of a monotonic function, in this case, χ^2. The routine is supplied with a function subroutine to calculate the function to be minimized. The final result is a rod length which is best suited to this particular choice of β and *baseline*. A slight change in β or *baseline* would produce a slightly different "best length". The second approach to estimate L was by a nonlinear fit to $g^{(2)}(t) - 1$ with β, *baseline*, and L as variables. This was achieved by adding the rod model, as described above (eq 11), to the analysis package GENDIST for the analysis of $g^{(2)}(t)$ data modeled on a $g^{(1)}(t)$ model. The advantages of this approach are twofold: the more obvious advantage is in achieving a universal optimization with respect to all three variables simultaneously. The second advantage is in the ability to compare this model fit with alternative fits performed using the same statistical weights. Judgments are made with respect to lack-of-fit (normalized residuals) and goodness-of-fit (reduced χ^2 and "quality parameter", Q).

Viscosity Measurements. Viscosity measurements were made using a capillary viscosimeter (Ubbelohde) in a temperature-controlled water bath. The investigated concentrations of P-85 in water were 0.10, 0.25, 0.50, and 1.0% (w/w). The outflow time of the solutions was measured in the temperature range 40–85 °C. Water was used as a reference. For dilute solutions the relative viscosity can be approximated to

$$\eta_{rel} \approx t/t_0 \quad (12)$$

where t and t_0 are the times of outflow for the solution and water, respectively. The solution viscosities were obtained by multiplying eq 12 by the water viscosity at the corresponding temperature.

Results and Discussion

Viscosity. A sphere-to-rod transition should increase the viscosity. Figure 1 shows the absolute solution viscosity plotted as a function of temperature for four P-85 concentrations together with the water viscosity. At 70 °C a strong increase of the viscosity with concentration is observed for the three higher concentrations measured. These results are in excellent agreement with low shear viscosity measurements made previously on the same sample batch.[11] The 0.10% curve in the diagram represents the lower limit of resolution in comparison to the water curve. These results suggest that the micelles change shape in this concentration regime on increasing the

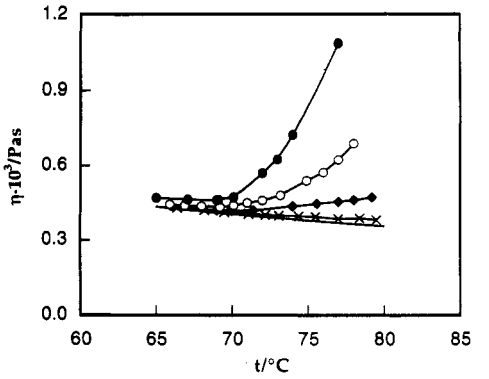

Figure 1. Sphere-to-rod transition. The viscosity of P-85 in water as a function of temperature at different concentrations: 0.10% (w/w) (×), 0.25% (w/w) (◆), 0.50% (w/w) (○), and 1.0% (w/w) (●). Water was measured as a reference (solid line). The lines are guides for the eye.

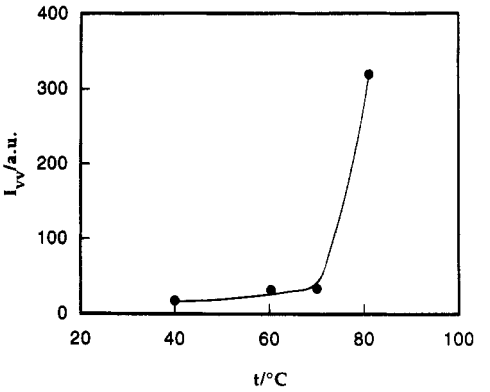

Figure 2. Sphere-to-rod transition. The polarized scattered intensity at $\theta = 90°$ is plotted as a function of temperature for a solution of 1.0% (w/w) P-85 in water. The line is a guide for the eye.

temperature. The increase in viscosity in this temperature region has also been examined using oscillatory shear viscosity measurements[25] and by determining the restriction in movement of a magnetic bar[26] (although not below a concentration of 2% (w/w)) together with intrinsic viscosity measurements.

Polarized Dynamic Light Scattering. To unambiguously estimate the rod length it is necessary to work at very high dilution, but still above the critical micelle concentration, to minimize frictional interactions between particles. Dramatic changes commence in the system at a temperature around 70 °C: the polarized scattered intensity increases strongly, a depolarized scattering component appears, and the solution viscosity increases substantially. The relaxation time distributions of polarized DLS measurements also change from single modal[13] to bimodal with the appearance of a rotational component in the spectrum of scattered light. These changes are consistent with a marked departure of the micellar shape from spherical symmetry. For highly asymmetric molecules, such as rods of sufficient length, rotational diffusion coefficients may be measured with the dynamic light scattering technique, and thereby the length of the micelles can in principle be estimated. Polarized (VV) dynamic light scattering measurements were made on different concentrations of P-85 in water in the range 0.025–1.0% (w/w) and at different angles between 50 and 120°. Figure 2 shows the increase in the scattered polarized intensity, I_{VV}, as a function of temperature for a dilute solution, which follows the same trend as the viscosity data in Figure 1. Preliminary static light scattering measurements (SLS), with a laser wavelength of 633 nm, on solutions of 0.050,

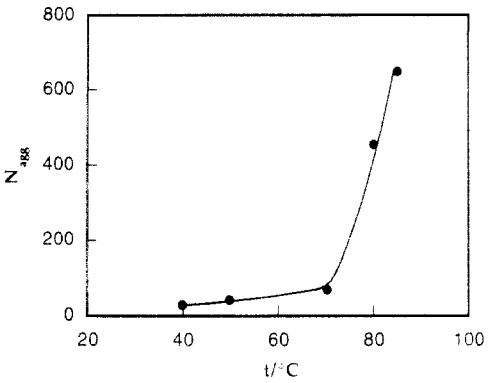

Figure 3. Micellar growth. The aggregation number from SLS (M_{mic}/M_{mon}) of the P-85 micelles is plotted as a function of temperature. The line is a guide for the eye.

0.10, 0.50, and 1.0% (w/w) P-85 in water at the temperatures 70, 80, and 85 °C showed no or little significant angular dependence over the angular range $35 < \theta < 145°$. From the micellar molecular weights, M_{mic}, an aggregation number, N_{agg}, of the micelles could be determined by dividing M_{mic} by the monomeric molecular weight, M_{mon} = 4600 g/mol. The aggregation numbers at 40 and 50 °C have been taken from earlier SLS measurements.[13] The temperature dependence of N_{agg} is displayed in Figure 3 and shows an increasing micellar growth. The temperature dependence of the SLS data gives an aggregation number of 255 at 75 °C.

Figure 4a shows a typical measured intensity autocorrelation function for a 0.025% (w/w) solution of P-85 in water at $\theta = 120°$. The data are also displayed in Figure 4b in the form of a logarithm–linear diagram. The corresponding relaxation time distribution, obtained by regularized inverse Laplace transformation (RILT) of the correlation function, is displayed in Figure 4c. As anticipated from eqs 1 and 11, the distribution was bimodal at the angles used and consisted of a small-amplitude fast peak and a large-amplitude slow peak with the relaxation rates Γ_f and Γ_s, respectively. The fast peak corresponds to a composite of rotational relaxation and translational diffusion and the slow peak to translational motion, according to eqs 1 and 11. The relaxation rates, obtained from the moments of the peaks in the relaxation time distribution, and the relative amplitudes are given in the output of the RILT program. For the concentration of 0.025% (w/w) the relative amplitude ($\tau A(\tau)$) of the fast peak was 2.5% at $\theta = 120°$ and 2.1% at $\theta = 50°$.

To assess the reproducibilities of the peak positions obtained in the RILT analysis, multiple determinations were made on the 1.0% (w/w) solution. This gave $\log(\tau_f/\mu s) = (1.62 \pm 0.14)$ at $\theta = 70°$. The variance/$\langle\Gamma\rangle^2$ of the translational peak in the relaxation time distributions obtained from RILT analysis was approximately 0.015 (average over the different q values) for the different concentrations. The value indicates a low polydispersity. However, due to possible anisotropic translation, the apparent polydispersity is probably smaller when estimated from the dispersion of the translational peak than is actually the case.

It may be pointed out that, with increasing qL, higher exponential terms in eq 1 become significant. The rotational peak will then include higher rotational modes superimposed in the relaxation time distribution.[27,28]

Estimation of the Rod Length. It is realized that the P-85 micelles at higher temperaures may not form completely inflexible rods of uniform length. They may have significant flexibility and also be polydisperse. Thus

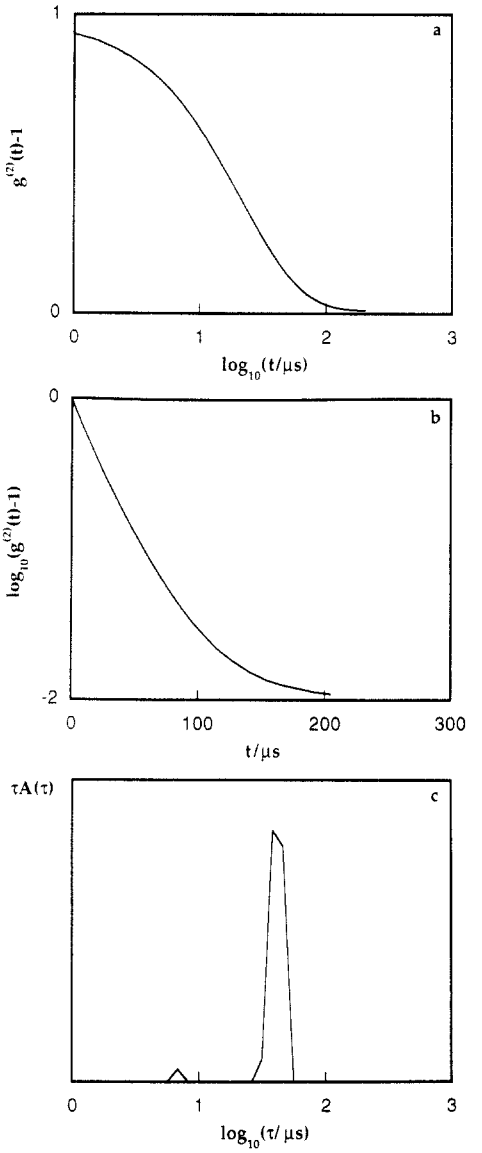

Figure 4. (a) Autocorrelation function of polarized scattered light (VV) at $\theta = 120°$ (b) Plot in (a) with logarithmic y axis and linear x axis. (c) The corresponding relaxation time distribution obtained from regularized inverse Laplace transformation of the autocorrelation function for a solution of 0.025% (w/w) P-85 in water at 75 °C. The fast peak is related to the rotational motion and the slow peak to the translational motion of the rodlike micelle.

the model to be used is uncertain and complex. However, for the present purpose of demonstrating that extended structures are formed at the higher temperatures and to obtain an approximate estimation of their length, the simple rod model has been chosen in preference to a more elaborate description incorporating flexibility and rotational–translational coupling. As the results will show, however, the rigid rod model probably does not grossly overestimate the length and is to a first approximation the best choice. It is also shown that the high relative intensities in the polarized geometry strongly favor such measurements in preference to those in the depolarized geometry, although both types of measurement yield similar results.

For the different concentrations of P-85 the micellar rod length L, was estimated in two ways:

Method I. In Figure 5, the two relaxation rates, extracted by RILT of the polarized DLS data, are plotted as a function of the square of the scattering vector, q^2, for a P-85 concentration of 0.050% (w/w). The other con-

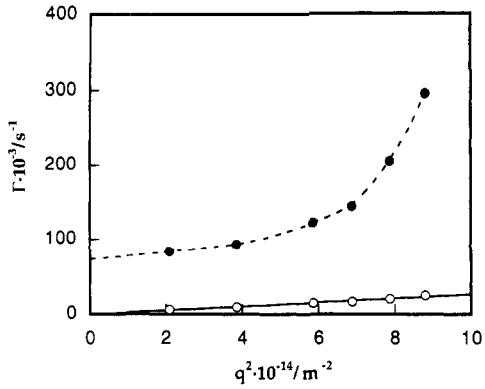

Figure 5. The two relaxation rates extracted from regularized inverse Laplace transformation of the polarized DLS data as a function of the squared scattering vector for a P-85 concentration of 0.050% (w/w). The relaxation rate for the slower mode is linear in q^2 (○) and the slope (from the linear least squares fit) is the translational diffusion coefficient. The rotational diffusion coefficient is related to the value of the fast rate (●) at $q = 0$ (intercept with the y axis). The broken line is a guide for the eye.

Table 1. Comparison of Measured and Calculated Parameters for P-85 in Dilute Aqueous Solution at 75 °C

c/(% (w/w))	$D \times 10^{12}$/ (m²/s)	$\Theta \times 10^{-3}$/ s⁻¹ [a]	L_I/Å [b] min–max	R_H/Å [c]
0.025	27.3	13.3	1050–1160	247
0.050	26.5	12.3	1090–1200	255
0.10	21.8	6.00	1470–1590	
0.50	20.8	4.50	1640–1790	
1.0	21.3	4.17	1710–1850	

c/(% (w/w))	$D_{rod} \times 10^{12}$/ (m²/s) [d]	L_{II}/Å [e] min–max	R_g/Å [f]
0.025	28.2 ± 0.3	770–1170	310
0.050	26.5 ± 0.4	890–1350	320
0.10	19.9 ● 0.9	1500–2260	
0.50	19.5 ± 0.8	1560–2320	
1.0	21.3 ± 0.6	1350–1980	

[a] Equation 3. [b] Method I, with $r = 75$ Å (min) and with $r = 50$ Å (max). [c] Equation 14 with measured D. [d] Equation 5 with L_{II}—the limits are given using $r = 50$ Å and $r = 75$ Å, respectively. [e] Method II, with $r = 75$ Å (min) and with $r = 50$ Å (max). [f] Equation 17 with L_I (min) and $r = 75$ Å.

centrations showed a similar pattern. The relaxation rate of the slow component, Γ_s, of the correlation function is linear in q^2 and the slope is identified as the translational diffusion coefficient, D, of the single rod. The translational diffusion coefficients for the different concentrations are given in Table 1. As an independent check of the correctness of the RILT results, the DLS data were also fitted to two exponentials, using a double-exponential function (see eq 10), and good agreement was found.

Figure 6 depicts fast relaxation rates, Γ_f, for the two highest concentrations, 0.50 and 1.0% (w/w). The data can be approximated by a common curve over this very limited range in concentration. The rotational diffusion coefficient, Θ, is obtained by extrapolating the relaxation rate for the low-amplitude fast mode, Γ_f, to scattering vector $q = 0$ for each concentration since $(\Gamma_f)_{q=0} = 6\Theta$ (see eq 3).

In Figure 7, the rotational diffusion coefficient is shown as a function of P-85 concentration. To estimate the length of the micelles, eq 4 was used with d set to twice the hydrodynamic radius of the spherical micelle, $R_H = 75$ Å determined earlier,[29] and using L as the fitting parameter. This procedure results in Figure 8. The Θ values for the various concentrations are collected in Table 1 with the obtained lengths (L_I) of the rod.

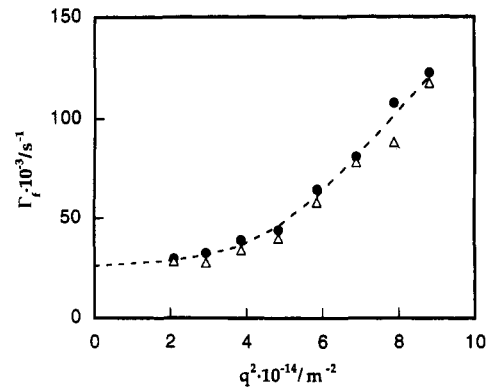

Figure 6. The relaxation rate of the fast rotational mode from regularized inverse Laplace transformation of the polarized DLS data as a function of the squared scattering vector for the concentrations 0.50% (w/w) (●) and 1.0% (w/w) (△) at 75 °C. The line is a guide for the eye.

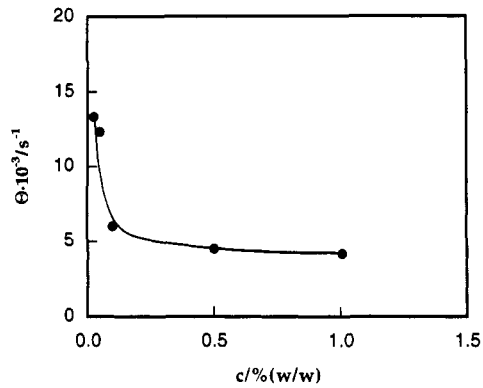

Figure 7. Rotational diffusion coefficient as a function of P-85 concentration at 75 °C. The line is a guide for the eye.

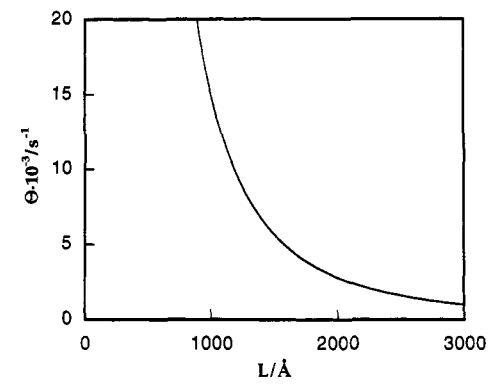

Figure 8. Theoretical prediction for the variation of the rotational diffusion coefficient of a rigid rod of radius 75 Å with its length at 75 °C (eq 4).

By using the R_H from DLS measurements as the maximum radius of the rod and the core radius $R_c = 50$ Å at 70 °C from SANS measurements[9] as the minimum radius, two extreme values of the length of the rod may be estimated (Table 1). The smaller the radius of the rod, the longer the rodlength. For the concentration of 0.025% (w/w), a mean value of 1110 Å is obtained from the two L_I values. The apparent length change on increasing concentration, seen in Table 1, is most likely the result of increasing interaction (see below).

The fast component increases more strongly with increasing scattering vector than would be expected for a rod of $L \approx 1000$ Å since the higher order terms in eq 1 contribute only weakly. A possible cause of the strong curvature is that the distributions are not as narrow as

anticipated and scattering from larger particles contributes significantly.

Method II. The rod length for a specific concentration was also obtained by fitting a constructed intensity autocorrelation function based on the normalized electric field correlation function for a rodlike particle (eqs 1 and 11) to the experimental data. The FORTRAN program used is described in more detail under Data Analysis. Fitting was made using the GENDIST package (see Appendix), where the program with the rod model is included as one of the fitting models. From the best fit between the rod model and the measured intensity autocorrelation function, with L, β, and the *baseline* as variables, the two extreme L values were extracted (L_{II} in Table 1). Each L_{II} value is therefore an average over the different angles, and this may be compared with the L value (L_I) obtained in method I. From Table 1, it can be seen that the values are rather close. In the dilute limit (c = 0.025% (w/w)), the mean value of the different L_{II} values in Table 1 is 970 Å.

Broersma's equation for the translational diffusion coefficient, eq 5, has also been used to calculate a theoretical D value, D_{rod}, at the different concentrations using the L_{II} values extracted from the best fit of the rod model to the data. Measured and calculated D values are given in Table 1. The D values are rather close to each other at the lowest concentrations, which supports a rodlike structure.

More Concentrated Solutions. Three concentration regimes may be defined for rodlike molecules of length L and diameter d:[30]

(a) The dilute regime is the region in which the solution contains an isotropic distribution of noninteracting rods, free to rotate. In this regime, the number concentration of rods, c_n, is $\ll 1/L^3$.

(b) The semidilute region is defined as the region $1/L^3 \ll c_n \ll 1/dL^2$. The rods are still isotropically distributed. The only restriction is that the rods cannot pass through each other, which inhibits rotational motion. Rotation and translation are strongly coupled.

(c) The concentrated region corresponds to $c_n > 1/dL^2$.

In the semidilute range, the rotational diffusion coefficient will have a very strong length and concentration dependence. The concentration dependence of the rotational diffusion coefficient has been shown to be given by[30,31]

$$\Theta = \beta' \frac{\Theta_0}{L^6 c_n^2} \tag{13}$$

where β' is a proportionality constant, c_n is the number concentration of rods, and Θ_0 is the rotational diffusion coefficient at infinite dilution.

A plot of Θ versus $1/c^2$ is shown in Figure 9 for the present data. It is seen that the onset of the semidilute regime occurs somewhat above 0.050%, and beyond this concentration the plot of Θ versus $1/c^2$ is linear. Zero and Pecora[18] find qualitatively similar behavior for solutions of poly(γ-benzyl L-glutamate) in 1,2-dichloroethane. The value of L (L_I) deduced above at the different concentrations (Table 1) will thus be a simple measure of the rod dimension only for the lowest concentration used (mean value 1110 Å). The average value from the rod model fit (L_{II}) is 970 Å.

It is noted that theory predicts that D will be reduced to half its infinite dilution value in the semidilute range. Here an approximately 20% reduction in D is found over the concentration range used, which indicates the crossover to the semidilute regime.

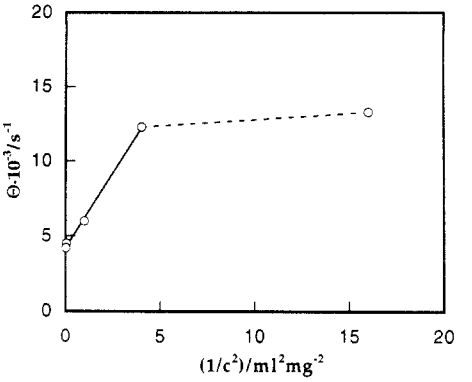

Figure 9. The semidilute region. The rotational diffusion coefficient at 75 °C is plotted versus the reciprocal concentration squared of P-85, showing the onset (linear relationship) of the semidilute region. The line is a linear least squares fit of Θ versus $1/c^2$ for $1/c^2 < 4$. The broken line is a guide for the eye.

A small diffusional anisotropy may be estimated using eqs 6a and 6b. For c = 0.025% (w/w), $D_\parallel = 26.6 \times 10^{-12}$ m²/s and $D_\perp = 23.6 \times 10^{-12}$ m²/s using L_I = 1050 Å.

Translational Diffusion. The equivalent hydrodynamic radius, R_H, was evaluated using the measured translational diffusion coefficient, D, at a concentration of 0.025% (w/w) using the Stokes–Einstein relationship:

$$R_H = \frac{kT}{6\pi\eta_0 D} \tag{14}$$

The result, 247 Å, can be compared with the value calculated using the formula for a rod:[32]

$$R_H = \frac{L}{2\sigma - 0.19 - 8.24/\sigma + 12/\sigma^2} \tag{15}$$

with $\sigma = \ln(L/r)$, where L = 1050 Å (l_I, Table 1) and r = 75 Å. This equation gives R_H = 285 Å.

Alternatively, Perrin's formula[33] for a prolate ellipsoid of semimajor axis a and semiminor axis b can be used:

$$R_H = \frac{a\sqrt{1-(b/a)^2}}{\ln\left[\frac{1+\sqrt{1-(b/a)^2}}{b/a}\right]} \tag{16}$$

With $a/b = (2/3)^{1/2}L/d$, where $a = L/2$ and $d = 2r$,[34] R_H = 213 Å is obtained. The experimental value (247 Å) lies between the value for a rod and a prolate ellipsoid. Using L = 770 Å (L_{II}, Table 1) in eqs 15 and 16 gives R_H values of 245 and 177 Å, respectively.

Assuming a rodlike shape, the radius of gyration, R_g, can be calculated using the L_1 and r values as above by means of the standard relationship

$$R_g = \left(\frac{L^2}{12} + \frac{r^2}{2}\right)^{1/2} \tag{17}$$

This gives R_g = 310 Å. The finding that the ratio $\rho = R_g/R_H$ is low (≅1.25) reflects the fact that the rod is short and bulky ($L/d \cong 7$). A homogeneous sphere would have ρ = 0.778 and a long thin rod $\rho > 2.0$.[35] Maeda and Fujima[36] have derived expressions for the correlation function and relaxation time for semiflexible rods incorporating the Kuhn statistical segment length, γ, which in turn is related to the persistence length P by $\gamma = (1/2P)$. With L the length of the macromolecule, the Gaussian coil limit corresponds to $\gamma L \gg 1$, and in the rigid rod limit $\gamma L \ll 1$.

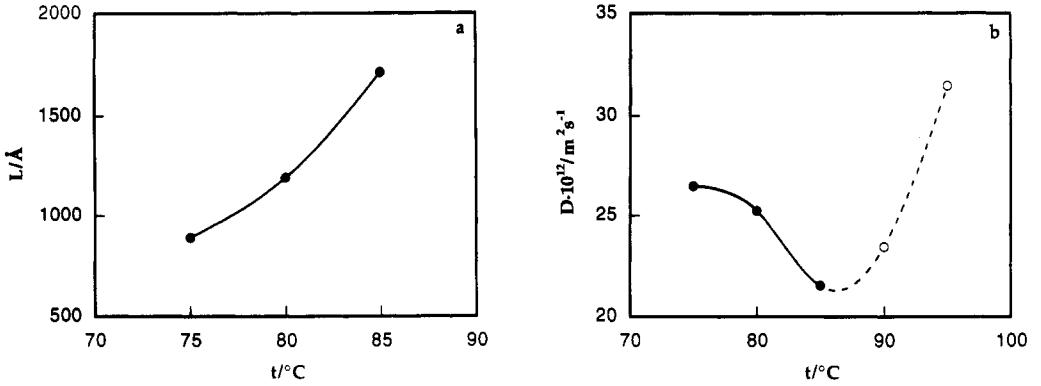

Figure 10. Temperature dependence. The rod length obtained from method II (with r = 75 Å) (a) and the translational diffusion coefficient (extracted from the slope of $\Gamma_s = f(q^2)$) (b) for a P-85 concentration of 0.050% (w/w) in water are plotted as a function of temperature. The filled circles represent the temperatures at which both translational motion and rotational motion are present. At the temperatures with open circles only translational motion is seen. The lines are guides for the eye.

Using the relationship[31,37]

$$R_g^2 = P^2\left[(L/3P) - 1 + 2(P/L) - 2\left(\frac{1-\exp(-L/P)}{(L/P)^2}\right)\right] \quad (18)$$

for R_g and inserting R_g = 310 Å and L = 1050 Å (Table 1), a value $\gamma L \approx 10^{-2}$ is extracted, implying proximity to the rigid rod limit.

It is noted that Flamberg and Pecora[38] studied the conformation of the highly extended micelles of dodecyldimethylammonium chloride (DDAC) at high ionic strength and concluded that large flexible rodlike micelles are present. A value of γL = 2.8 was found in this case.

The experimental value for the rotational relaxation time for c = 0.025% (w/w) is γ_1 = 25 μs employing $2/\tau_1 = 6\Theta$ in the rod limit. Using the expression for a Gaussian coil, $\tau_1 = (2R_g^2/D\pi^2)$, gives τ_1 = 7.1 μs, which is considerably faster than the experimental value. Use of the Maeda and Fujima model[36] in the rigid rod limit with $\tau_1 = 1.2\text{-}(L^2/27D)$ gives τ_1 = 18 μs. The difference between this value and the experimental figure of 25 μs will mainly be due to the influence of frictional interactions at finite concentration.

Temperature Dependence. The temperature dependence of the rod length and the translational diffusion coefficient of a concentration of 0.050% (w/w) was examined; see Figures 10a and 10b, respectively. At 75, 80, and 85 °C a rotational mode was present, indicating rodlike particles. The rod length could therefore be estimated from the rod model (L_{II}) at those temperatures. As shown in Figure 10a, the length is increasing with temperature, which is also indicated as a decreasing translational diffusion coefficient in Figure 10b. At 90 °C, however, which is on the verge of clouding, only the translational peak is observed and the diffusion coefficient increases.

Depolarized Dynamic Light Scattering. At around 70 °C the micellar solutions show significant depolarized scattering, I_{VH}. The depolarized component of the scattered light spectrum is due to the anisotropic part of the optical polarizability of the macromolecular component in solution, which may derive from two sources: (a) the optical anisotropy[39] of the components of the copolymer itself and (b) if the former are optically isotropic, from the nonspherical shape of the micelle.[40] In the case of P-85, composed of PEO and PPO, it may be assumed that both the monomers and the micelles are isotropic and that the depolarized scattering is only due to the form anisotropy of the micelle. This conclusion can be drawn from the fact that I_{VH} is negligible at temperatures at which spherical micelles are present but increases to become significant around 70 °C, where the sphere-to-rod transition starts.

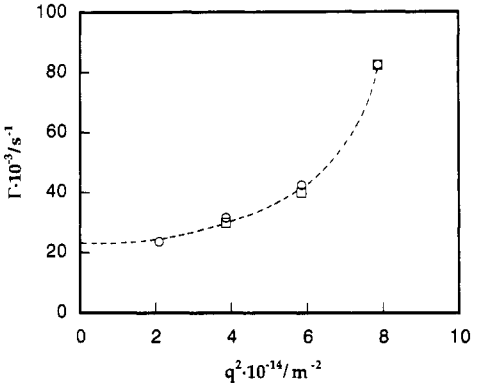

Figure 11. Comparison between polarized (VV) and depolarized (VH) DLS. The fast relaxation rate from polarized DLS (○) and the single relaxation rate from depolarized DLS (□) are plotted as a function of the squared scattering vector for a 1.0% (w/w) solution of P-85 in water at 75 °C. The line is a guide for the eye.

In the VH geometry, only the scattering due to the optical anisotropy of the rod is collected, which leads to a single-modal distribution with relaxation frequency $\Gamma_{VH} = (q^2D + 6\Theta)$ in the low-angle limit, identical to the fast relaxation frequency, Γ_f, extracted from the polarized experiment after RILT of the data. The depolarized electric field correlation function is

$$g^{(1)}_{VH}(q,t) = A\exp(-\Gamma_{VH}t) + \textit{baseline} \quad (19)$$

The depolarized intensity is, however, always very low (typically of the magnitude 4 kHz with 900-mW laser power). The measurements thus required longer duration. Adjustment of the analyzer with extreme care was necessary in the present case since the polarized intensity was very high and would otherwise leak through. This situation strongly favors the approach used above (methods I and II) where the polarized intensity is sufficiently high to give precision even for the low relative amplitude of the rotational/translational component.

In principle, the depolarized experiment may be made at zero angle, but the leakage problem is then severe; the measurements were thus made at a series of higher angles. As in the case of the fast mode isolated using RILT of the polarized DLS data, the rotational diffusion coefficient is determined using eq 3 to correct for q^2D. A comparison

between $\Gamma_f(VV)$ and the single mode, Γ_{VH}, is shown for the data at a series of q vectors in Figure 11.

At higher concentrations and temperatures, a hexagonal phase is formed, one of the properties of which is optical birefringence. SAXS measurements show that such a liquid crystalline phase exists at a P-85 concentration of 43% (w/w) at 70 °C.[41] This has also been shown by optical microscopy.[15] Therefore, a check of the occurrence of birefringence in P-85 solutions of intermediate concentration (15, 20, 25, 27.5, and 30% (w/w)) and 75 °C and above has been made by placing the sample between a crossed polarizer and an analyzer. Flow birefringence describes a solution that becomes birefringent under shear stress due to the ordering of long rods.[30] This may occur at concentrations already below the boundary to the hexagonal phase. The results show that the boundary to the hexagonal phase is not sharp. Thus at 75 °C, 15, 20, and 25% (w/w) are flow birefringent and 27.5% (w/w) is on the verge of the hexagonal phase since it is birefringent without shear but the intensity of the transmitted light increases on shearing. The 30% (w/w) solution is in the hexagonal region.

These results show that rodlike micelles are present at 75 °C which interact increasingly as the concentration is increased until the hexagonal phase is formed.

Acknowledgment. We are grateful to G. Svensk for making the viscosity measurements. This work was supported by the Swedish Natural Science Research Council (NFR) and the Swedish National Board for Technical Development (NUTEK).

Appendix

GENDIST is an interactive program for the analysis of homodyne DLS data. The program will fit three different models: a *form free* model and a *fixed form* model for the distribution for relaxations and a *fixed form* for the intensity autocorrelation function. All the models include an adjustable *baseline* and an adjustable β.

1. The *form free fit* to relaxations entails laying out a grid of possible relaxation times, evenly spaced on a logarithmic axis, and determining, by a least squares procedure, the best positive amplitudes on this grid. A second-order regularizer is introduced to produce smoothing of the spiky distribution. This is similar, in principle, to the operation of CONTIN,[42,43] but, unlike CONTIN, it operates directly on the $g^{(2)}(t)$ function rather than the $g^{(1)}(t)$ function. In addition, the calculation algorithm has been altered to increase the speed considerably, and the desired *probability to reject* may be set for the direct computation of this level of smoothing. This algorithm is due to J. Jakeš in Prague, and is termed REPES (REgularized Positive Exponential Sum).[21]

2. The *fixed form* calculation model uses a nonlinear least squares algorithm to fit either a single asymmetric broad peak distribution in relaxation times (called GEX),[44] a single symmetrical broad peak distribution (called GAUSS), or the composite sum of GEX and GAUSS peaks.

3. The *fixed form* intensity autocorrelation function is the Williams–Watts stretched exponential (or the sum of two such stretched exponentials).

References and Notes

(1) Al-Saden, A. A.; Whateley, T. L.; Florence, A. T. *J. Colloid Interface Sci.* **1982**, *90*, 303–309.
(2) Rassing, J.; Attwood, D. *Int. J. Pharm.* **1983**, *13*, 47–55.
(3) (a) Zhou, B.; Chu, B. *Macromolecules* **1987**, *20*, 3089–3091. (b) Zhou, B.; Chu, B. *Macromolecules* **1988**, *21*, 2548–2554. (c) Zhou, B.; Chu, B. *J. Colloid Interface Sci.* **1988**, *126*, 171–180.
(4) Wanka, G.; Hoffmann, H.; Ulbricht, W. *Colloid Polym. Sci.* **1990**, *268*, 101–117.
(5) Elias, H. G. In *Light Scattering from Polymer Solutions*; Huglin, M. B., Ed.; Academic Press: London and New York, 1972; pp 397–448.
(6) Tuzar, Z.; Kratochvíl, P. *Adv. Colliod Interface Sci.* **1976**, *6*, 201–232.
(7) Linse, P. *Macromolecules* **1993**, *26*, 4437–4449.
(8) Fleischer, G. *J. Phys. Chem.* **1993**, *97*, 517–521.
(9) Mortensen, K.; Pedersen, J. S. *Macromolecules* **1993**, *26*, 805–812.
(10) Linse, P. *J. Phys. Chem.* **1993**, *97*, 13896–13902.
(11) Glatter, O.; Scherf, G.; Schillén, K.; Brown, W. *Macromolecules*, to be published.
(12) Vadnere, M.; Amidon, G.; Lindenbaum, S.; Haslam, J. L. *Int. J. Pharm.* **1984**, *22*, 207–218.
(13) Brown, W.; Schillén, K.; Almgren, M.; Hvidt, S.; Bahadur, P. *J. Phys. Chem.* **1991**, *95*, 1850–1858.
(14) Mortensen, K. *Europhys. Lett.* **1992**, *19*, 599–604.
(15) Tiddy, G. J. T., unpublished results.
(16) Pecora, R. *J. Chem. Phys.* **1968**, *48*, 4126–4128.
(17) (a) Broersma, S. *J. Chem. Phys.* **1960**, *32*, 1626–1631. (b) Broersma, S. *J. Chem. Phys.* **1960**, *32*, 1632–1635. (c) Broersma, S. *J. Chem. Phys.* **1981**, *74*, 6989–6990.
(18) Zero, K. M.; Pecora, R. *Macromolecules* **1982**, *15*, 87–93.
(19) Russo, P. S. In *Dynamic Light Scattering*; Brown, W., Ed.; Oxford University Press: Oxford, 1993; pp 512–553.
(20) Reddy, N. K.; Fordham, P. J.; Attwood, D.; Booth, C. *J. Chem. Soc., Faraday Trans.* **1990**, *86* (9), 1569–1572.
(21) Jakeš, J. *Czech, J. Phys.* **1988**, *B38*, 1305–1316.
(22) Nicolai, T.; Brown, W.; Johnsen, R. M.; Štěpánek, P. *Macromolecules* **1990**, *23*, 1165–1174.
(23) Johnsen, R. M. In *Laser Light Scattering in Biochemistry*; Harding, S. E., Sattelle, D. B., Bloomfield, V. A., Eds.; The Royal Society of Chemistry: Cambridge, 1992; pp 77–91.
(24) For a discussion of the Golden Section Search, as well as a program listing for the algorithm, see *Numerical Recipes in FORTRAN: The Art of Scientific Computing*, 2nd ed.; Press, W. H., Teukolsky, S. A., Vetterling, W. T., Flannery, B. P., Eds.; Cambridge University Press: New York, 1992; pp 390–395.
(25) Hvidt, S., personal communication.
(26) Bahadur, P.; Pandya, K.; Almgren, M.; Li, P.; Stilbs, P. *Colloid Polym. Sci.* **1993**, *271*, 657–667.
(27) Nicolai, T.; Brown, W.; Johnsen, R. M. *Macromolecules* **1989**, *22*, 2795–2801.
(28) Brown, W. *Macromolecules* **1985**, *18*, 1713–1719.
(29) Schillén, K.; Glatter, O.; Brown, W. *Prog. Colloid Polym. Sci.* **1993**, *93*, 66–71.
(30) Doi, M.; Edwards, S. F. *The Theory of Polymer Dynamics*; Oxford University Press: Oxford, 1986.
(31) Tracy, M. A.; Pecora, R. *Annu. Rev. Phys. Chem.* **1992**, *43*, 525–557.
(32) Young, C. Y.; Missel, P. J.; Mazer, N. A.; Benedek, G. B.; Carey, M. C. *J. Phys. Chem.* **1978**, *82*, 1375–1378.
(33) Chu, B. *Laser Light Scattering*; Academic Press: London, 1974; p 212.
(34) Tanford, C. *Physical Chemistry of Macromolecules*; John Wiley & Sons: New York, 1961; p 342.
(35) Burchard, W. In *Laser Light Scattering in Biochemistry*; Harding, S. E., Sattelle, D. B., Bloomfield, V. A., Eds.; The Royal Society of Chemistry: Cambridge, 1992; pp 3–22.
(36) Maeda, T.; Fujima, S. *Macromolecules* **1981**, *14*, 809–818.
(37) Allison, S. A.; Sorlie, S. S.; Pecora, R. *Macromolecules* **1990**, *23*, 1110–1118.
(38) Flamberg, A.; Pecora, R. *J. Phys. Chem.* **1984**, *88*, 3026–3033.
(39) Pecora, R. *J. Chem. Phys.* **1968**, *49*, 1036–1043.
(40) Fytas, G.; Patkowski, A. In *Dynamic Light Scattering*; Brown, W., Ed.; Oxford University Press: Oxford, 1993; pp 440–470.
(41) Glatter, O., to be published.
(42) Provencher, S. W. *Comput. Phys. Commun.* **1982**, *27*, 213–227.
(43) Provencher, S. W. *Comput. Phys. Commun.* **1982**, *27*, 229–242.
(44) Nicolai, T.; Brown, W.; Hvidt, S.; Heller, K. *Macromolecules* **1990**, *23*, 5088–5096.